Mode Specificity in Reactions of Cl with CH_2 Stretch-Excited $CH_2D_2(v_1, v_6 = 1)$[†]

Jens Riedel,[‡] Shannon Yan,[§] and Kopin Liu*

Institute of Atomic and Molecular Sciences (IAMS), Academia Sinica, P.O. Box 23-166, Taipei, Taiwan 10617

Received: March 24, 2009; Revised Manuscript Received: April 25, 2009

We report on a reactive scattering experiment of chlorine atom (Cl) with mode-selected *dideutero*-methane (CH_2D_2) using a pulsed crossed beam approach with a time-sliced velocity-map imaging detection of the methyl radical products. Reactivity with one-quantum excitation of CH_2D_2 in either CH_2 symmetric ($\nu_1 = 1$) or antisymmetric ($\nu_6 = 1$) stretching mode are contrasted over a wide range of collisional energies, as well as compared to the recently reported reaction dynamics of the ground-state reactants. We found that the vibrational excitation in either stretching mode leads to a nearly identical enhancement factor in total reactivity, which is also comparable to an equivalent amount of additional translational energy. On the other hand, the correlated HCl vibrational distributions from reactions of the two stretch-excited CH_2D_2 reactants exhibit a distinct mode-specificity. Overall, the observed behaviors bear strong resemblance to the mode-dependent reactivity reported recently for reactions of Cl + $CH_4(\nu_3 = 1)$ and Cl + $CHD_3(\nu_1 = 1)$. The dynamical implications are elucidated and plausible mechanisms proposed.

I. Introduction

Beyond its relevance in the atmospheric ozone cycle,[1] the hydrogen-atom transfer between methane and chlorine atom has become a benchmark system for understanding the influence of reactant vibration excitations on a polyatomic reaction. It is now well documented, both experimentally[2−17] and theoretically,[18−24] that excitation of different vibrational motions of a polyatomic reactant can exert profound effects on chemical reactivity. An intuitively appealing picture emerges from these mode-selective studies: The nuclei motions resulting from excitation of a mode with a large displacement along a particular reaction coordinate can preferentially drive the system over the transition state along that coordinate, leading to mode-dependent reactivity and product branching ratios.

However, many fascinating questions remain unanswered and need deeper understanding. For example, in a series of pioneering works on the dynamical effects of symmetric (ν_1) and antisymmetric (ν_3) stretch excitations of CH_4 in Cl + CH_4,[6−8] Zare and co-workers found both stretching excitations yielding in virtually identical product internal state distributions and angular distributions. On the basis of these observations, they concluded that the initial preparation of CH_4 in different stretching modes may or may not alter the total reactivity, the dynamics leading to product formation, however, follow a common pathway, along which the initial mode character gets scrambled by vibrational mixing during the collision event. In those studies, the absolute reactivity enhancements of the two stretching modes could not be determined because of the difficulty of quantifying the relative excitation efficiencies by an infrared (IR) absorption for $CH_4(\nu_3 = 1 \leftarrow 0)$ and a stimulated Raman pumping of the IR-inactive $CH_4(\nu_1 = 1 \leftarrow 0)$ transition. That difficulty was alleviated by Crim and co-workers in studying the relative reactivity of Cl atom with excited symmetric C−H stretch (ν_1) and antisymmetric C−H stretch (ν_4) excitations of CH_3D, for which both stretching modes can be activated by direct IR excitations with quantified efficiencies.[12,13] A noticeable difference in reactivity was observed: $\sigma(\nu_1 = 1) = 4.4 \times \sigma(\nu_4 = 1)$. On the basis of this finding, they proposed a vibrationally adiabatic model,[12,13,24] in which the approach of the Cl atom causes the vibrational energy of the CH_3D symmetric and antisymmetric stretches to become localized in the proximal and distal C−H bonds, respectively. Thanks to this collision-induced normal-to-local mode evolution or an intramolecular vibration energy redistribution (IVR) process, the symmetric stretch contains more energy along the reaction coordinate, leading to a higher reactivity than that of the antisymmetric stretch excitation. In other words, the reaction remains largely vibrationally adiabatic without significant state mixing between the two local modes during a reactive collision. Despite the fact that the above two reactions involve different isotopomers, the subtle differences between the two proposed viewpoints remain to be reconciled.

Complementary to those findings, very recently we contrasted the reaction of Cl atom with the symmetric CH stretch-excited $CHD_3(\nu_1 = 1)$[15,16] against the antisymmetric stretch-excited $CH_4(\nu_3 = 1)$.[17] Next to striking similarities, the results also exposed some distinct differences between the individual reactions. We found that exciting a specific mode does not affect the total reactivity, except at very low collision energies, and, even more surprisingly, the same rate-enhancement factor can be achieved by an equivalent amount of extra translational excitation. The character of the excited mode does, on the other hand, have profound effects on the product state distribution. These results, however, were for stretch excitation of different isotopes and thus could also stem from the accompanying subtle mass effects.

More pertinent to the present isotopic reaction are the two recent studies. The first is the remarkable report by Zare and co-workers on the bond and mode selectivity of the title reaction with overtone-excited CH_2D_2.[9,10] They found that excitation of the first C−H overtone of CH_2D_2 promotes only the H-atom abstraction reaction, and excitation of the first C−D overtone

[†] Part of the "Vincenzo Aquilanti Festschrift".

* To whom correspondence should be addressed. E-mail: kliu@po.iams.sinica.edu.tw.

[‡] Present address: Fritz-Haber-Institut der Max-Planck-Gesellschaft, Faradayweg 4-6, 14195 Berlin, Germany.

[§] Present address: Department of Chemistry, University of California, Berkeley, CA 94720, USA.

10.1021/jp902629h © 2009 American Chemical Society
Published on Web 05/29/2009

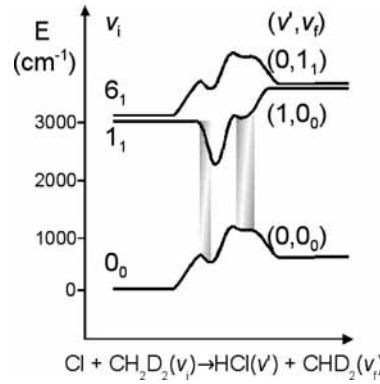

Figure 1. Schematic view of a cut-through of the vibrationally adiabatic potential-energy surfaces along the reaction coordinate. The shapes of the potential curves are qualitatively sketched in accord with previous ab initio calculations. Note that, whereas the Born−Oppenheimer potential-energy surface is smooth, the generalized vibrational frequencies orthogonal to the reaction coordinate can vary along the reaction path. As a result, the vibrationally adiabatic curves exhibit hills and valleys. On the basis of the previous theoretical predictions, two shaded regions indicate where the vibrationally nonadiabatic transitions (i.e., both the curvature and Coriolis couplings) may occur. The relevant states of this study are indicated. See text for detailed explanations.

of CH_2D_2 leads preferentially to the C−D bond cleavage. In addition, excitation of different modes, either two quanta in one C−H oscillator or a local mode containing one quantum each in two C−H oscillators, produces vastly different product state and angular distributions. The major findings of these bond- and mode-selective investigations can be summarized by an intuitively simple spectator model,[9,10] in which the Cl atom interacts with the single C−H oscillator and the remainder of the methane molecule does not participate in the reaction. The other report is the pair-correlated study of the ground-state reaction leading to the formation of $CHD_2(v = 0)$ and $CH_2D(v = 0)$.[25] Product pair-correlated excitation functions, vibrational branching ratios, and angular distributions were measured over a wide range of collision energies, from 2 to 22 kcal mol^{-1}. In addition, significant spin−orbit reactivity of $Cl^*(^2P_{1/2})$ was discovered and the effect of low-lying hot bands of CH_2D_2 reactants on reactivity was elucidated. The present investigation, in conjunction with the above two studies of the ground-state[25] and overtone-excited reactions,[9,10] then forms a rather comprehensive set of experimental data on the reaction dynamics of $Cl + CH_2D_2$.

Depicted in Figure 1 is a cut-through of the relevant potential-energy surfaces along the reaction coordinate as the Cl atom attacks one of the H atom. The shapes of the potential curves are sketched in rough accord with previous ab initio calculations,[18,19] and the vibrational-state correlations between the reactant and the product are based on symmetry grounds. It can be seen that $Cl + CH_2D_2(\nu_1 = 1)$ correlates to $(1, 0_0)^{\ddagger}$, whereas $Cl + CH_2D_2(\nu_6 = 1)$ should predominantly lead to the $(0, 1_1)^{\ddagger}$ formation. [The notation of the product state-pair is as follows. The first number gives the number of vibrational quanta in the HCl coproduct, whereas the second indicates the vibrational state in the methyl radical; and the double-dagger superscript denotes a vibrationally excited CH_2D_2 reactant.] Experimentally, we found that, contrary to the vibrationally adiabatic correlation shown in Figure 1, vibrationally hot methyl products constitute only minor to the overall flux. This report will therefore focus on the predominant ground-state methyl products; hereafter, for brevity the 0_0 notation will be omitted. Equivalent results for the remaining reaction channels leading to various vibrationally excited methyl products will be reported elsewhere in the future.

II. Experimental Section

The experimental setup has been described in detail elsewhere.[15,26,27] Briefly a doubly skimmed molecular beam of pure CH_2D_2, expanded from an EL pulsed valve[28] under a stagnation pressure of 6 bar at 20 Hz, was crossed by another doubly skimmed beam carrying Cl atoms. The latter was produced by a pulsed high-voltage discharge in the output of a molecular beam expansion of ~5% Cl_2 in helium/neon at 6 bar. The initial collision energy was tuned by changing the intersection angle of the two molecular beams. The nascent methyl products CHD_2 or CH_2D were probed by (2 + 1) resonance-enhanced multiphoton ionization (REMPI)[29−31] near 333 nm followed by a time-sliced velocity-map imaging detection scheme.[26] Whereas this approach allows an interrogation of the complete product state distribution; as mentioned above, this article will focus only on the predominant formation of methyl radical in its ground state (0_0). The ground-state products CHD_2 and CH_2D were probed respectively at the two-photon frequencies (in vacuum) of 59 921 cm^{-1} and 59 940 cm^{-1}, corresponding to the 0_0^0 Q-branch band head of the $3p^2B_1 \leftarrow X^2B_1$ transition.[25,30,31] The accumulation time was typically 2−5 h (adding up to about 1.5×10^5 to 3.5×10^5 events) depending on the individual signal strength.

A comment on the use of imaging technique in crossed-beam scattering experiments will be reiterated here. The raw image corresponds to the product density being probed, whereas the desired quantity is the reactive flux; thus, the image analysis requires a density-to-flux transformation. In practice, as detailed previously,[26] we first generated, thanks to the time-sliced approach, a 2D density-to-flux sensitivity matrix by explicitly accounting for the spatial and temporal overlaps of the two pulsed molecular beams, the timing and the focusing dependence of the REMPI process, the laboratory-velocity dependence of the detection sensitivity, and the time-slicing effects. The corrected flux-image was then transformed from the raw image and the sensitivity matrix through a pixel-by-pixel operation, and further analysis ensues.

To prepare a vibrationally excited CH_2D_2 reactant beam, we found that the use of the original (single-passage) setup yielded merely a few percents of excitation efficiency, in sharp contrast to earlier experiments on the other isotopomers in which the same amount of IR laser fluence could excite ~20% into $CHD_3(\nu_1 = 1)$ or $CH_4(\nu_3 = 1)$.[15−17] To pump up more CH_2D_2 into $\nu_1 = 1$ (2988.1 cm^{-1}) or $\nu_6 = 1$ (3012.2 cm^{-1}), the IR output from a seeded Nd:YAG pumped narrow-band OPO/OPA system (LaserVision) was sent through the methane beam just in front of the first skimmer, either twice using a prism retro-reflector (for most of the $\nu_1 = 1$ excitation data) or later through a multipass ring-reflector (for $\nu_6 = 1$).[32] The chosen wavelength was set using a photoaccoustic (PA) cell, as well with an action spectrum of the crossed-beam reaction of CH_2D_2 with fluorine atom by probing the $CHD_2(\nu_1 = 1)$ product, as a reference. The spectroscopic complexity of the antisymmetric rotor CH_2D_2[33] hampered an exact assignment of the PA spectrum; however, a coinciding peak in the PA signal with high ion intensity in the action spectrum indicated that the chosen transition originates from a low-lying j-state. Whereas the relative positions of the chosen transitions could be directly obtained from the PA spectrum of CH_2D_2, a small amount of CH_4 for which the spectrum is well understood[34] was added to the PA cell as an internal reference for the absolute IR frequency.

Even after IR exposure, most of the CH_2D_2 molecules still remain unexcited; therefore, the raw data acquired for the excited reactants constitute some contributions from ground-state

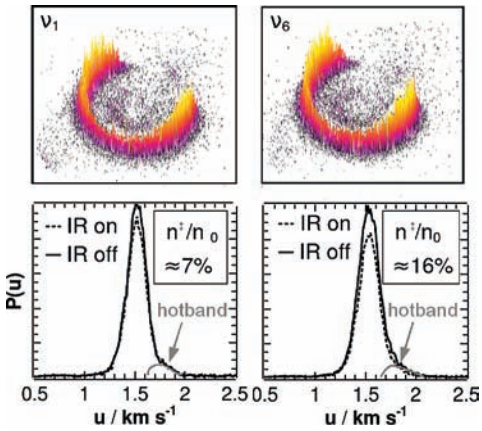

Figure 2. (Color) Top panels: Time-sliced velocity maps of the CH_2D products from the Cl + CH_2D_2 reaction. Bottom panels: The recoil velocity distributions P(u) with and without IR exposure. Note that IR-excitation does not lead to formation of any new features but merely depletes the $CH_2D(0_0)$ ground-state production.

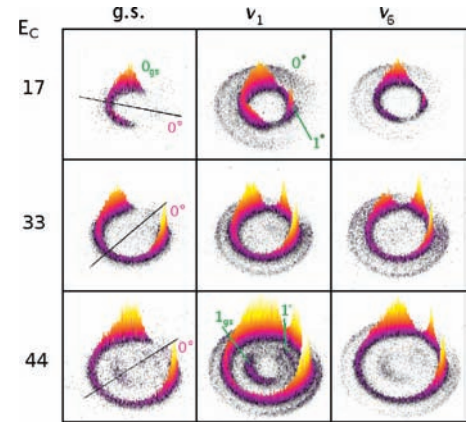

Figure 3. (Color) Raw images of the $CHD_2(0_0)$ products from the three different reactions: left column for Cl + $CH_2D_2(0_0)$, middle column for Cl + $CH_2D_2(\nu_1 = 1)$, and right column for Cl + $CH_2D_2(\nu_6 = 1)$, illustrated at three different collision energies E_c (in kJ mol^{-1}). The symbols 0° inside the left panels refer to the forward scattering direction of the nascent CHD_2 product. The state label refers to the vibrational quantum number of the HCl coproduct, with the subscript gs and the superscript of ≠ for the ground and stretch-excited reactants, respectively. The HCl($\nu = 1$) product from reaction with the spin−orbit excited of chlorine Cl* is indicated by 1*. The disparity of the image intensity mostly arises from the different accumulation time of each individual image.

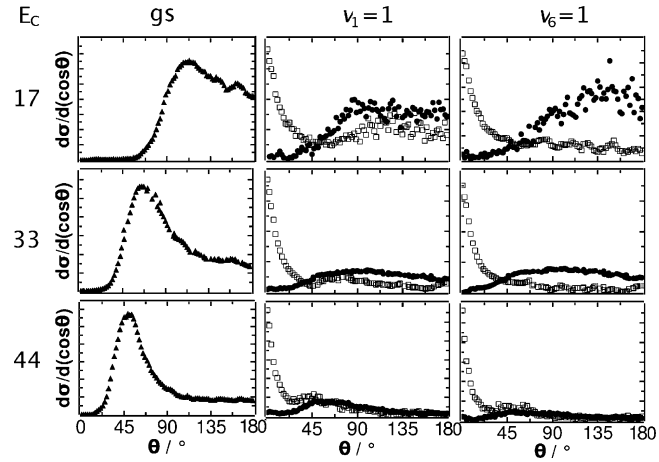

Figure 4. Angular distributions of the individual reaction channels of the images shown in Figure 3. For $\nu_1 = 1$ and $\nu_6 = 1$, the solid circles are for $0^‡$ and open circles for $1^‡$.

reactants. To analyze the observed images, the precise knowledge of the fraction of excited CH_2D_2 being pumped *and* contributing to the scattering signals, $n^‡/n_0$ as defined previously,[35] is needed. To this end, both the threshold method[35] and the depletion approach[32] were used. Whereas both methods yielded consistent results, the latter was found to be more convenient experimentally. As shown in Figure 2, in the D-atom transfer channel of this reaction the IR excitation leads to no additional image features ascribable to the formation of the ground-state CH_2D product; instead its signal gets bleached by the fraction of excited CH_2D_2 in the beam. Hence, by alternately measuring the amounts of depleted $CH_2D(0_0)$ products with and without IR exposure, the fraction of excited CH_2D_2 reactants, $n^‡/n_0$, can be determined.[32] The typical values in this study are $n^‡/n_0 = \sim 7\%$ using the earlier retro-reflector prism setup for Cl + $CH_2D_2(\nu_1 = 1)$, and ~16% for Cl + $CH_2D_2(\nu_6 = 1)$ when the multipass ring-reflector was implemented. [A few data points in the Cl + $CH_2D_2(\nu_1 = 1)$ reaction were double checked using multipass ring-reflector with $n^‡/n_0 = \sim 20\%$.] It is worth noting that the observation of suppressing the D-atom transfer channel upon the CH_2 stretch excitations of CH_2D_2 corroborates with the results by Zare and co-workers,[9,10] who found that upon the two-quanta excitation the CH stretch-excitation remains in the molecule as a mere spectator during CD bond fission and vice versa.

III. Results and Discussion

A. Correlated Product Angular Distributions. Exemplified in Figure 3 are a few time-sliced raw images of CHD_2 products thus obtained at three collision energies. The images of the ground-state reaction (left panel) nicely resemble results published earlier,[25] and the observed single sharp ring energetically corresponds to the formation of CHD_2 product in the vibrational ground state. Hereafter, we will refer this channel to 0_{gs} with the subscript gs denoting the products being formed from the ground-state reactants and the zero corresponding to the quanta in the correlated HCl molecule. [As aforementioned, this article only concerns the ground-state $CHD_2(0_0)$ product, and its vibrational quantum excitation is omitted.] As can be seen in Figure 4, the product angular distribution of this channel is predominantly backward at low collision energies and becomes more sideways with increasing collision energy. This behavior is well understood as a direct scattering process through the peripheral reaction mechanism.[36−40]

In both vibrationally excited images, $\nu_1 = 1$ (center panel) and $\nu_6 = 1$ (right panel), two additional features arise. The most obvious is a second ring with a broad distribution peaking at larger radii. Energetically, these CHD_2 products can readily be assigned to the ground-state products formed out of vibrationally excited reactants $0^‡$ (i.e., the same notation as above only the double dagger indicates vibrationally excited methane). Second, the shape of the inner ring changes drastically and an additional product peak toward the forward direction can be observed. Because the vibrational frequencies of the CH stretch in methane and the HCl stretch are similar, the added reactant's vibration energy could be balanced by the additional product excitation of HCl($\nu = 1$), yielding a nearly same recoil velocity as that of 0_{gs}. Hence, the additional forward peak is attributed to HCl($\nu = 1$) when $CHD_2(0_0)$ is probed, denoting as $1^‡$. Moreover, the distribution of the pure 0_{gs} is known from the IR-off image and its contribution to the inner ring of IR-on images can be accounted for by scaling the IR-off distribution by $(1 - n^‡/n_0)$,[35] as such the superimposed pure $1^‡$ distribution can be

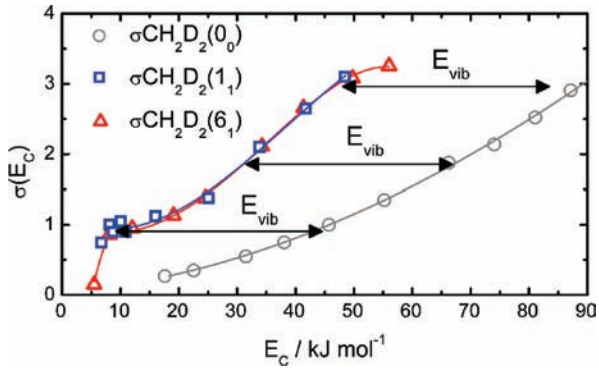

Figure 5. (Color) Excitation functions of the vibrationally excited reactants CH_2D_2, $\nu_1 = 1$ (in blue squares) and $\nu_6 = 1$ (in red triangles), along with the previously reported ground-state behavior (in gray) for comparison. The horizontal bars indicate the amount of additional vibration energy deposited in the molecules to allow a comparison between collisional and vibrational excitement. Note that even at the lowest collisional energies of this study both stretch-excited reactants lead to a finite amount of reactive fluxes but clearly differ in the amounts.

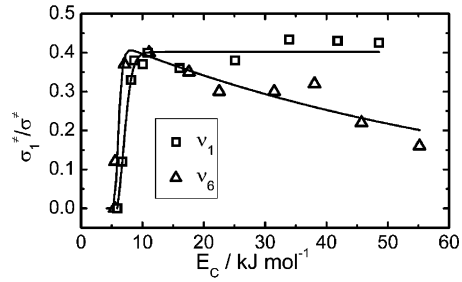

Figure 6. E_c evolution of the vibrational branching fractions of the correlated HCl products, $\sigma_1^{\ddagger}/\sigma^{\ddagger}$, for both stretch-excited reactions.

reconstructed. The resultant angular distributions of the two stretch-excited CH_2D_2 reactions are also depicted in Figure 4, which show a strong similarity, albeit some subtle differences, of the two cases.

The angular distributions for the $0^{\ddagger}$ channel in both stretch-excited reactions are strikingly similar and show the typical trend of a direct scattering process, that is, predominantly backward scattering at lower E_c, followed by sideways and more forward scatterings at higher E_c. Compared to the ground-state reaction,[25] this peripheral character appears somewhat less pronounced. Similar behaviors were found previously in the reactions of Cl + $CHD_3(\nu_1 = 1)$[15,16,35] and Cl + $CH_4(\nu_3 = 1)$.[17] On the other hand, the $1^{\ddagger}$ distributions exhibit a bimodal character: A sharp forward feature is superimposed on a broad component that appears to shift gradually toward smaller scattering angles with increasing collision energies. Again, similar behavior was previously noted in the Cl + $CHD_3(\nu_1 = 1) \rightarrow HCl(\nu = 1)$ + $CD_3(0_0)$ channel.[15,16] We interpreted the observation as a result of two competitive reaction pathways. Whereas a fraction of reactive events proceed by direct scattering, some other correlated $HCl(\nu = 1)$ are formed through a pathway involving a short-lived collision complex supported by the vibrationally adiabatic well, as depicted in Figure 1. It is intriguing to note that the E_c evolution of the broad component appears more pronounced for $\nu_1 = 1$ than for $\nu_6 = 1$.

B. Vibrational Enhancement in Reaction Rates. In Figure 4, the relative differential cross sections derived from a pair of IR-on and IR-off images at a given collision energy are normalized to each other. By integrating each distribution over all angles (weighted by the solid-angle factor sin θ) and accounting for the $n^{\ddagger}/n_0$ factor of the excited reactant concentrations, the respective vibrational enhancement factor at each E_c can be obtained. In conjunction with the previously reported excitation function of the ground-state reaction,[25] the excitation functions for the stretch-excited CH_2D_2 reaction can then be derived. Figure 5 summarizes the results for the stretch-excited reactants $CH_2D_2(\nu_1 = 1)$ and $CH_2D_2(\nu_6 = 1)$, along with the previously reported excitation function of the ground-state reactant[25] for comparison.

Two remarks are in order. First, except at very low energy regime, $E_c < 10$ kJ mol^{-1}, the two stretch-excited excitation functions are essentially identical. In view of the facts that each of the data points was obtained from a pair of images (IR-on and IR-off) over a period of months and that the IR pumping efficiencies of the two modes on each day and for different optical setups were somewhat different, this result is quite remarkable and robust. The implication of this finding is obvious: the symmetry of the two stretching modes does not appear, except at very low E_c, to be crucial to the vibrational enhancement of the reaction rate.

Second, also marked in the figure are a few horizontal lines indicating equivalent vibration energies. Inspecting the excited- and ground-state excitation functions, it becomes apparent that at lower E_c both CH_2-stretching excitations are somewhat less efficient (but significantly more so at very low E_c) than an equivalent translational energy in promoting the reaction rate and at higher E_c the vibration becomes slightly favored. Nonetheless, this differential preference in promoting the reactivity by vibration or translation is subtle and perhaps not as large as one might have initially thought for a reaction with the productlike transition state.[18−22] In other words, it is by and large the amount − not the forms − of energy in governing the promotion of the reactivity.

C. Mode Specificity of Correlated Vibration Branching of Product Pairs. The excitation functions shown in Figure 5 refer to the total reactive fluxes of $CHD_2(0_0)$ that is the dominant methyl product in the Cl + $CH_2D_2(\nu_1$ or $\nu_6 = 1)$ reaction. The 2D character of the velocity-map imaging approach provides further insights into the HCl coproduct state distribution and thus a distinction between the two $(0, 0_0)$ and $(1, 0_0)$ channels. Figure 6 presents the correlated HCl vibration branching fraction of $(1, 0_0)/[(0, 0_0) + (1, 0_0)]$, that is $\sigma_1^{\ddagger}/\sigma^{\ddagger}$. As can be seen in both cases, the branching fractions rise sharply to about 0.4 once the individual threshold for the $(1, 0_0)$ channel is reached. As the collisional energy increases, $\sigma_1^{\ddagger}/\sigma^{\ddagger}$ for Cl + $CH_2D_2(\nu_6 = 1)$ displays a monotonic decline to about 0.2 at $E_c = \sim 55$ kJ mol^{-1}, whereas that for Cl + $CH_2D_2(\nu_1 = 1)$ remains constant. Interestingly, this mode-symmetry-dependent finding is reminiscent of similar behaviors reported recently for the other two isotopically analogous reactions. In the case of Cl + $CHD_3(\nu_1 = 1)$, the symmetric CH-stretching excitation led to an E_c-independent $\sigma_1^{\ddagger}/\sigma^{\ddagger} = \sim 0.44$,[15] for an antisymmetric stretch-excited reaction of Cl + $CH_4(\nu_3 = 1)$ a declining vibration branching fraction with E_c was found.[17]

D. Correlated Energy Disposal. The different behaviors of mode-specific vibration branching fraction point to different energy disposals of the two reactions. The question is: As the collisional energy increases, what kind of product excitation will the additional energy flow into? The CHD_2 REMPI detection is state-selective so only the HCl rotation and the total kinetic energy release (KER) can compensate for the HCl vibrational excitation. Figure 7 shows how much energy is deposited as KER ($T^{\ddagger}$) or in the correlated HCl motions, E_{vib} ($V^{\ddagger}$) and E_{rot} ($R^{\ddagger}$), respectively. Because both $V^{\ddagger}$ and $T^{\ddagger}$ are directly obtained from analyzing the image, $R^{\ddagger}$ can then be

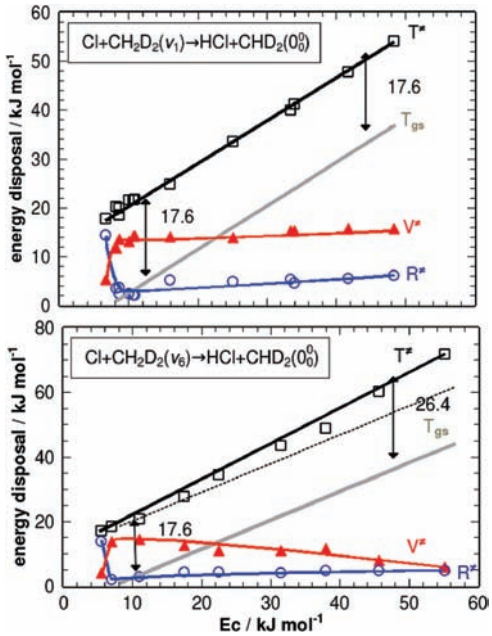

Figure 7. (Color) Correlated energy disposals of the title reactions. See text for details.

deduced by conservation of energy. The upper panel shows that in the $CH_2D_2(\nu_1 = 1)$ reaction both the vibrational and the rotational energies of the correlated HCl remain roughly constant, whereas the increasing available energy is mainly channeled into translation, resulting in a linear dependence of $T^{\ddagger}$ on E_c. Also depicted in the figure is the KER of the ground-state reaction, which has been shown previously to follow extremely well the prediction of a simple kinematic model, T_{gs}.[38,40] Interestingly, the E_c dependence of $T^{\ddagger}$ is simply shifted upward from that of T_{gs} by a constant value of 17.6 kJ mol^{-1}, which is about 50% of the initial vibration excitation energy.

Similar analysis was performed for the $Cl + CH_2D_2(\nu_6 = 1)$ reaction and the results presented in the lower panel. Obviously, $V^{\ddagger}$ declines with increasing E_c, as expected from the vibrational branching fraction shown in Figure 6, and $R^{\ddagger}$ again remains constant. So, the excessive energy flows into $T^{\ddagger}$ at a faster pace than the increase in E_c, ranging from about 50% of initial vibration energy at low E_c to more than 75% at higher E_c. In other words, the vibrational energy stored in the initial ν_6 mode of excitation gets transformed into product translation more effectively than an equivalent amount that stored in ν_1, yet not leading to an increase of the overall reactivity.

E. Proposed Interpretations and Reaction Mechanism. Similar to the two different viewpoints from different isotopic reactions mentioned in the Introduction, the results of this study in the same isotopic reaction also suggest two seemingly conflicting views of the underlying reaction pathways and mechanisms. On the one hand, nearly identical vibrational enhancement factors (or excitation functions, again, except at very low E_c) for $Cl + CH_2D_2(\nu_1 = 1)$ and $Cl + CH_2D_2(\nu_6 = 1)$ could arise from a common reaction pathway for the two stretch-excited reactions. On the other hand, the distinct E_c dependencies of the vibrational branching fraction of the two stretch-excited reactions would implicate different reaction mechanisms, in contrast to the mutual reaction pathway.

To reconcile the apparent paradox, we first noted that significant vibrational nonadiabaticity must occur in the two stretch-excited reactions; otherwise, by the vibrational correlation depicted in Figure 1, the $Cl + CH_2D_2(\nu_1 = 1)$ reaction would have yielded the $(1, 0_0)$ pair as the major products and the $Cl + CH_2D_2(\nu_6 = 1)$ reaction should have led to significant production of $CHD_2(\nu_1 = 1)$, in sharp contrast to the experimental observation. In fact, the striking similarity of the two stretch-excited excitation functions corroborates well with the picture of a strong mixing of the two modes in the reaction entrance valley. However, the way of this mode mixing is to be in contrast to the recently proposed vibrationally adiabatic model,[12,13,24] which is essentially a local mode picture. In that model the approach of the Cl atom dephases the two normal modes and would have caused the vibrational energy of the CH_2D_2 symmetric (ν_1) and antisymmetric (ν_6) stretches to become localized in the proximal (reactive) and distal (unreactive) C−H bonds, respectively, thus, leading to a differential reactivity of the two modes.

Then, what is the nature of the mode mixing and what does happen in the transition-state region for the initially prepared $\nu_1 = 1$ and $\nu_6 = 1$ reactions? The transition state of the $Cl + CH_2D_2 \rightarrow HCl + CHD_2$ reaction is believed to be of collinear Cl−H−C configuration;[18,19] thus, the minimum energy path should maintain the C_{2v} symmetry. Moreover, ab initio calculations of the isotopically analogous reactions[12,13,18−22] indicated a strong curvature coupling (i.e., coupling induced by the curvature of the reaction path) of the $\nu_1 = 1$ mode to the reaction coordinate near the transition state, as illustrated by the shaded regions in Figure 1, resulting in a significant decrease of the generalized vibration frequency. In contrast, $\nu_6 = 1$ mode is of b_1 symmetry in the C_{2v} configuration, which cannot couple directly to the reaction coordinate through the curvature coupling, resulting in a nearly invariant vibration frequency along the reaction path and the spectator behavior of that mode if the reaction would have proceeded vibrationally adiabatically.

Asymptotically, theoretical study of the vibrations of CH_2D_2 indicated that the normal-mode descriptions of the two stretching modes are a fairly good approximation, ~100% of purity for $\nu_6 = 1$ and ~94% for $\nu_1 = 1$ (the remaining ~6% is mainly two-quantum excitation of the CH_2-scissor mode ν_3), respectively.[41,42] However, as the Cl atom approaches, the mode characters will be perturbed by the long-range intermolecular interactions. In the C_{2v} configuration, a mode of b_1 symmetry can Coriolis-couple to an a_1 species such as the $\nu_1 = 1$ mode due to the anisotropic interactions. Hence, the ν_1/ν_6 mode mixing in the entrance valley is likely mediated through the collision-induced Coriolis interactions (i.e., the intermode mixings induced by the twisting of the transverse vibrations about the curved reaction path as the reaction proceeds). If this mode-mixing occurs prior to the entrance barrier of the ν_1-excited curve shown in Figure 1, which is presumably the reaction bottleneck, one might argue that the comparable reactivity of the initially prepared $\nu_6 = 1$ reactants toward the Cl atom comes from the reactivity borrowing of mixing in the ν_1-mode characters. We noted in passing that the two reactants are heavy, thus the interaction time needed for the long-range mode mixings can be significant. For example, during the 11 fs of vibrational period for ν_1 or $\nu_6 = 1$, the trajectory moves only 0.013 nm (or 0.031 nm) at $E_c =$ 8 kJ mol^{-1}(or 50 kJ mol^{-1}). Therefore, over the energy range of this study the Cl atom would always sample several vibrational periods during the long-range encounter, allowing time for mode mixing.

Yet, the fact that the initial excitations of the two modes exhibit different dynamical attributes, such as the correlated vibration branching fraction (see Figure 6), implies the above simple ν_1/ν_6 mode-mixing does not completely scramble their memory, underscoring the necessity of more detailed mecha-

nisms. In analogy to the previous findings of the Cl + $CHD_3(\nu_1 = 1)$ reaction,[16] we envision that other low-frequency modes such as ν_3 (the CH_2 scissor) and ν_4 (CD_2 scissor), which are also of the a_1 species and generally behave as a transitional mode (namely transforming into the translational and rotational motions of the departing products),[15,16] might actively partake, allowing the initially prepared ν_6 excitation to couple to the reaction coordinate in a different way from the ν_1 excitation.

In other words, the picture we proposed is as follows. Whereas the approach of Cl atom could cause a collision-induced vibrational energy redistribution (IVR) to mix the $\nu_1 = 1$ and $\nu_6 = 1$ modes at long-range, the initially prepared mode character is to some extent retained prior to the transition-state region. As the reaction proceeds, the colliding pair with initial ν_1-excitation experiences a strong curvature coupling, near the first shaded regime in Figure 1, by funneling the energy into the reaction coordinate and the reactive trajectories bifurcate. Those retained in the initial excitation within the Cl−H−C moiety will be trapped by the vibrational-adiabatic (dynamical) well, forming a short-lived reaction complex, and eventually lead to the $(1, 0_0)$ product pair. This accounts for the observed sharp forward feature in the product angular distribution. The other bifurcated pathway from the curvature coupling gives rise to vibrationally nonadiabatic transitions so that the reaction proceeds further over the ground-state surface and yields mainly the $(0, 0_0)$ product pair. This is the same reaction mechanism proposed previously for the Cl + $CHD_3(\nu_1 = 1) \rightarrow$ HCl + $CD_3(0_0)$ reaction.[15,16] In support of the above interpretation are the similar observations of an E_c-independent vibrational branching fraction of the correlated HCl products in two reactions and the distinct E_c evolution of the broad, direct components in the angular distribution of the $(1, 0_0)$ pair shown in Figure 4.[15] The latter attribute could arise from the couplings in the second (exit valley) shaded region, where some of the reactive fluxes (over the ground-state surface) could back-flow onto the vibrationally excited ν_1-surface to form the $(1, 0_0)$ pair.[16] Clearly, this path bypasses the dynamical well and will be, by and large, of a direct scattering path.

For reaction with initially prepared ν_6 excitation, it could, as aforementioned, strongly couple to the ν_3/ν_4 modes through the collision-induced Coriolis interactions prior to and near the first shaded region. Because the ν_3/ν_4 modes, as a transitional mode by nature,[16] can readily curvature-couple to the reaction coordinate,[15] thus again, the bifurcation of the reactive trajectories is expected to occur. Moreover, the collision-induced Coriolis interaction involves twisting the mode amplitudes; we thus assert it being impact-parameter dependent. As the collisional energy increases, larger impact-parameter collisions contribute to reaction and at the same time the collision-induced Coriolis interactions become stronger. As such, a larger fraction of bifurcated trajectories will undergo the vibrationally nonadiabatic transition onto the ground-state surface than those starting with $\nu_1 = 1$ reactants, resulting in the smaller vibration-excited branching fraction of HCl as observed. In that regard, we note that, at very low E_c, the impact-parameter-dependent Coriolis coupling is necessarily small, which may account for the smaller vibrational enhancement factor for ν_6 than the ν_1 excitation (Figure 5). In addition, the ν_3/ν_4 modes of excitation generally act as the transitional mode in a reaction by funneling the vibrational energy into the translational and rotational energy of the products.[16] By mixing the ν_3/ν_4 mode characters into the initially prepared ν_6 excitation, the couplings required for an efficient back-flow onto the excited ν_1-surface in the second shaded region will not be the same as that from the initially prepared ν_1 reactants. Hence, the observed subtle differences in angular distributions between $\nu_1 = 1$ and $\nu_6 = 1$ (Figure 4) would not be too surprising.

Consistent with previous studies,[12,13,15−17,43] the present results clearly indicate that intramolecular vibrational redistribution (IVR) takes place to various extents, depending on the isotopic substitutions, during the course of the reactions. The explanation of various observations for different reactions is necessarily complex and could have many causes. The interpretation and mechanisms proposed above are qualitative at the present stage and are not without pitfalls. First, the viewpoint is largely within the framework of reaction path Hamiltonian[44] and restricted to the minimum reaction pathway. Second, the arguments are drawn heavily upon the symmetry considerations. Although the reaction certainly occurs in the C_s configuration of the Cl−H−C moiety, we believe that the consideration at higher symmetry − C_{2v} in accord with the transition-state structure[18−22] − should bring out the propensity and capture the major features of the chemical reactivity. More serious and rigorous theoretical works will be needed to gain deeper insights into the experimental observations reported here and into the mode-specific reactivity in general.

IV. Conclusions

Using a time-sliced imaging technique under the crossed-beam condition, the reactivity and product state distributions of the reactions Cl + $CH_2D_2(\nu_1 = 1$ and $\nu_6 = 1)$ have been studied and elucidated. We found a nearly identical (vibrational) enhancement factor of the two reactant modes over a wide collisional energy range, yet very different behaviors in pair-correlated vibration-state distributions. Striking similarities and differences are also contrasted to the isotopically analogous reactions of Cl + $CHD_3(\nu_1 = 1)$ and Cl + $CH_4(\nu_3 = 1)$. To interpret the observations, we suggest that both stretch-excited reactions proceed through a similar (yet not identical) reaction mechanism, being governed by different mode-coupling behaviors in the transition-state region.

Acknowledgment. We are indebted to Drs. D. S. Wang and H. Kawamata for their help in some of the experiments. This work was financially supported by the National Science Council of Taiwan, Academia Sinica, and the U.S. Air Force Office of Scientific Research (AOARD-09-4030).

References and Notes

(1) Solomon, S. *Rev. Geophys.* **1999**, *37*, 275.
(2) Crim, F. F. *Acc. Chem. Res.* **1999**, *32*, 877.
(3) Zare, R. N. *Science* **1998**, *279*, 1875.
(4) Sinha, A.; Hsaio, M. C.; Crim, F. F. *J. Chem. Phys.* **1990**, *92*, 6333.
(5) Bronikowski, M. J.; Simpson, W. R.; Girard, B.; Zare, R. N. *J. Chem. Phys.* **1991**, *95*, 8647.
(6) Simpson, W. R.; Orr-Ewing, A. J.; Zare, R. N. *Chem. Phys. Lett.* **1993**, *212*, 163.
(7) Simpson, W. R.; Rakitzis, T. P.; Kandel, S. A.; Orr-Ewing, A. J.; Zare, R. N. *J. Chem. Phys.* **1995**, *103*, 7313.
(8) Bechtel, H. A.; Camden, J. P.; Brown, D. J. A.; Zare, R. N. *J. Chem. Phys.* **2004**, *120*, 5096.
(9) Kim, Z. H.; Bechtel, H. A.; Zare, R. N. *J. Am. Chem. Soc.* **2001**, *123*, 12714.
(10) Bechtel, H. A.; Kim, Z. H.; Camden, J. P.; Zare, R. N. *J. Chem. Phys.* **2004**, *120*, 791.
(11) Yoon, S.; Henton, S.; Zivkovic, A. N.; Crim, F. F. *J. Chem. Phys.* **2002**, *116*, 10744.
(12) Yoon, S.; Holiday, R. J.; Crim, F. F. *J. Phys. Chem. B* **2005**, *109*, 8388.
(13) Yoon, S.; Holiday, R. J.; Sibert III, E. L.; Crim, F. F. *J. Chem. Phys.* **2003**, *119*, 9568.
(14) Zhou, J.; Lin, J. J.; Zhang, B.; Liu, K. *J. Phys. Chem. A* **2004**, *108*, 7832.

(15) Yan, S.; Wu, Y. T.; Zhang, B.; Yue, X.; Liu, K. *Science* **2007**, *316*, 1723.
(16) Yan, S.; Wu, Y. T.; Liu, K. *Proc. Natl. Acad. Sci. U.S.A.* **2008**, *105*, 12667.
(17) Kawamata, H.; Tauro, S.; Liu, K. *Phys. Chem. Chem. Phys.* **2008**, *10*, 4378.
(18) Duncan, W. T.; Truong, T. N. *J. Chem. Phys.* **1995**, *103*, 9642.
(19) Corchado, J. C.; Truhlar, D. G.; Espinosa-Garcia, J. *J. Chem. Phys.* **2000**, *112*, 9397.
(20) Espinosa-Garcia, J. *J. Phys. Chem. A* **2007**, *111*, 5792–9654.
(21) Sanson, J.; Corchado, J. C.; Rangel, C.; Espinosa-Garcia, J. *J. Phys. Chem. A* **2006**, *110*, 9568.
(22) Martinez, R.; Gonzalez, M.; Defazio, P.; Petrongolo, C. *J. Chem. Phys.* **2007**, *127*, 104302.
(23) Schatz, G. C. *J. Chem. Phys.* **1979**, *71*, 542.
(24) Fair, J. R.; Schaefer, D.; Kosloff, R.; Nesbitt, D. J. *J. Chem. Phys.* **2002**, *116*, 1406.
(25) Wu, Y. T.; Liu, K. *J. Chem. Phys.* **2008**, *129*, 154302.
(26) Lin, J. J.; Zhou, J.; Shiu, W.; Liu, K. *Rev. Sci. Instrum.* **2003**, *74*, 2495.
(27) Lin, J. J.; Zhou, J.; Shiu, W.; Liu, K. *Science* **2003**, *300*, 966.
(28) Even, U.; Jortner, J.; Noy, D.; Lavie, N. *J. Chem. Phys.* **2000**, *112*, 8068.
(29) Brum, J. L.; Johnson III, R. D.; Hudgens, J. W. *J. Chem. Phys.* **1993**, *98*, 3732.
(30) Zhou, J.; Lin, J. J.; Liu, K. *J. Chem. Phys.* **2004**, *121*, 813.
(31) Zhou, J.; Lin, J. J.; Liu, K. *J. Chem. Phys.* **2003**, *119*, 8289.
(32) Riedel, J.; Yan, S.; Kawamata, H.; Liu, K. *Rev. Sci. Instrum.* **2008**, *79*, 033105.
(33) Ulenikov, O. N.; Hirota, E.; Akiyama, M.; Alanko, S; Koivusaari, M.; Anttila, R.; Geulachvili, G.; Tolchenov, R. N. *J. Mol. Spectrosc.* **1996**, *180*, 423.
(34) Brown, L. R.; Benner, D. C; Champion, J. P.; Devi, V. M.; Fejard, L.; Gamache, R. P.; Gabarrd, T.; Hilico, J. C.; Lavorel, B.; Loete, M.; Mellau, G. Ch.; Nikitin, A.; Pine, A. S.; Predoi.Cross, A.; Rinnsland, C. P.; Robert, O.; Sams, R. L.; Smith, M. A. H.; Tashkun, S. A.; Tyuterev, Vl. G. *J. Quant. Spectrosc. Radiat. Transfer* **2003**, *82*, 219.
(35) Yan, S.; Wu, Y. T.; Liu, K. *Phys. Chem. Chem. Phys.* **2007**, *9*, 250.
(36) Wang, X.; Ben-Nun, M.; Levine, R. D. *Chem. Phys.* **1995**, *197*, 1.
(37) Nyman, G.; Clary, D. G.; Levine, R. D. *Chem. Phys.* **1995**, *197*, 223.
(38) Zhou, J.; Zhang, B.; Lin, J. J.; Liu, K. *Mol. Phys.* **2005**, *103*, 1757.
(39) Zhang, B.; Liu, K. *J. Chem. Phys.* **2005**, *122*, 101102.
(40) Nyman, G.; Zhou, J.; Zhang, B.; Liu, K. *Isr. J. Chem.* **2007**, *47*, 1.
(41) Carter, S.; Shnider, H. M.; Bowman, J. M. *J. Chem. Phys.* **1999**, *110*, 8417.
(42) Wang, X.-G.; Sibert III, E. L. *J. Chem. Phys.* **1999**, *111*, 4510.
(43) Camden, J. P.; Bechtel, H. A.; Brown, D. J. A.; Zare, R. N. *J. Chem. Phys.* **2006**, *124*, 034311.
(44) Miller, W. H.; Handy, N. C.; Adams, J. E. *J. Chem. Phys.* **1980**, *72*, 99.

JP902629H